# Strain rate-induced phase transitions in an impact-hardening polymer composite

Weifeng Jiang, Xinglong Gong, Sheng Wang, Qian Chen, Hong Zhou, Wanquan Jiang, and Shouhu Xuan

Citation: Applied Physics Letters **104**, 121915 (2014); doi: 10.1063/1.4870044
View online: http://dx.doi.org/10.1063/1.4870044
View Table of Contents: http://scitation.aip.org/content/aip/journal/apl/104/12?ver=pdfcov
Published by the AIP Publishing

# Strain rate-induced phase transitions in an impact-hardening polymer composite

Weifeng Jiang,[1] Xinglong Gong,[1,a)] Sheng Wang,[2] Qian Chen,[1] Hong Zhou,[1] Wanquan Jiang,[2] and Shouhu Xuan[1]
[1]*CAS Key Laboratory of Mechanical Behavior and Design of Materials, Department of Modern Mechanics, University of Science and Technology of China (USTC), Hefei 230027, China*
[2]*Department of Chemistry, USTC, Hefei 230026, China*

(Received 27 February 2014; accepted 14 March 2014; published online 28 March 2014)

An impact-hardening polymer composite that is promising as a protective equipment material for its excellent performance and comfortable characteristics is shown. Falling weight impact experiments are performed to characterize its protective behavior, which is realized by absorbing energy and resisting deformation. From the mechanical tests in different strain rate, it is seen to undergo transitions from a viscous-liquid behavior to a rubbery behavior, then to a glassy behavior. These phase transition are found to be essential for their practical applications in the energy absorption and the deformation resistance. © *2014 AIP Publishing LLC*. [http://dx.doi.org/10.1063/1.4870044]

We might get injured in sports (rugby, motorcycle race, and skiing), natural disasters (earthquake, hurricane, and tsunami), dangerous work environments (building site, fire scene, and explosion), etc. In such cases, a super garment with resisting attacks and moving comfortably is needed. In the past decades, many materials have been used to prevent injury such as metals, ceramics, composites, and nanomaterials.[1–3] They can absorb a large amount of shock energy and retain structural integrity. However, they are heavy or hard. Liquid armor composited of ballistic fabrics and shear thickening fluid[4] have recently attracted much attention due to their excellent protection and comfort of wearing.[1,5,6] However, the sealing of the shear thickening fluid is challenging in the applications. Polymers with their stability, hardening with increasing rate and self-healing ability after impact[7] might be the ideal protective materials.[8] In particular, these polymers such as polyurethane, polyuria, and Silly Putty® caused their response to traverse the phase transition zone under impact have been widely exploited in the safety systems.[9–11] Here, an impact-hardening polymer composite (IHPC) with two stages of phase transitions is studied. It was observed to undergo transition from a viscous liquid behavior to a rubbery behavior, then to a glassy behavior with the increasing strain rate. Energy absorption and deformation resistance caused by the poly-phase transition make the IHPC have excellent performance of impact protection. Furthermore, because of the highly nonlinear behaviors of the IHPC, it is an ideal example to study the viscoelasticity of the polymers, and there are significant physical meanings within its "liquid-solid" transition related.

The IHPC was prepared as follows. First, simethicone, pyroboric acid, and a small amount of alcohol were placed into a beaker and heated under stirring for about 1 h at high temperature to obtain the raw rubber. Then, the raw rubber, benzoylperoxide and calcium carbonate were mixed uniformly in a mixing machine. In the last step, the IHPC was obtained by sulfurizing the mixing material by a baking oven. The IHPC appears milky white as shown in Fig. 1(a). In the normal case, it could be made into arbitrary shape desired and cold flow occurs under its own weight (Fig. 1(b)). If rolled into a ball and dropped, it showed a high elasticity. The rebound height was about 70%–80% of the drop height (Fig. 1(c)). In addition, if a hammer struck the IHPC, it instantly hardened and was not easy to deformation (Fig. 1(d)).

We used a falling weight system to study the protection behaviors of the IHPC under impact (Fig. 2(a)). During the test, impact mass strikes the IHPC with various drop heights. The instantaneous sensor signals including mass acceleration ($a$) and the bottom force ($F$) versus time are shown in Fig. 2(b). Rather than collapsing the IHPC, the mass pushes it down, suffering a stiff resistance. This immediately causes the peak contact force $F_c = m_{mass}a_{peak}$ (where $m_{mass}$ and $a_{peak}$

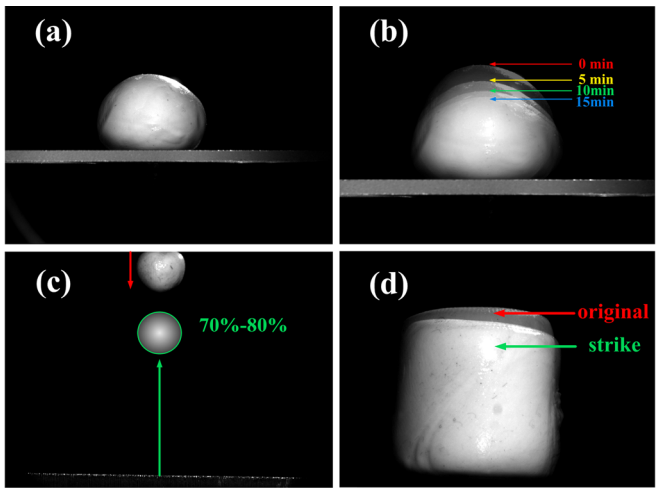


FIG. 1. Typical behaviors of an IHPC. (a) A piece of the IHPC. (b) Cold flow behavior of the IHPC, which is the tendency of the IHPC to move slowly under the influence of the stress like gravitation. It is a combination of four images (at various times 0 min, 5 min, 10 min, and 15 min). (c) High elasticity of the IHPC while free-falling. The rebound height is not readily captured. It is estimated by our observed value. (d) Deformation resistance of the IHPC under impact. It is a combination of two images (a hammer before and after striking the IHPC).

a)Electronic mail: gongxl@ustc.edu.cn

 

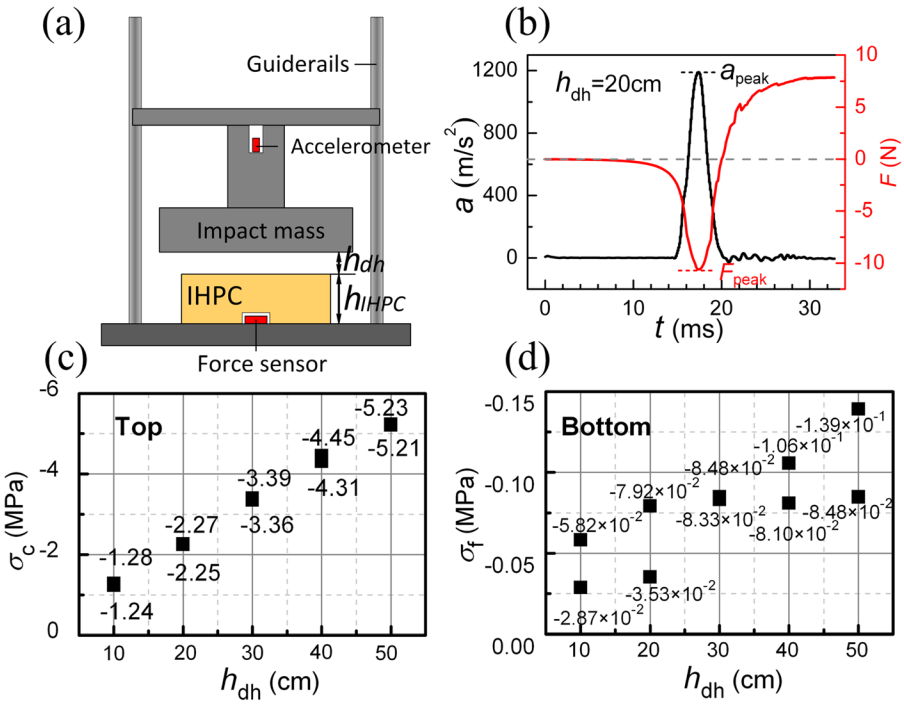


FIG. 2. Impact at the IHPC. (a) The impact mass ($m_{mass} = 2.4$ kg and $r_{mass} = 30$ mm) is housed by guiderails and launched via free-fall. Instantaneous mass acceleration $a$ is measured by an embedded accelerometer. A storeroom ($r_s = 14$ mm and $h_s = 4.5$ mm) is set directly below the IHPC ($r_{IHPC} = 25$ mm and $h_{IHPC} = 12$ mm). A force sensor ($r_f = 13$ mm and $h_f = 3$ mm) recorded the stress transmission to the bottom embed in the storeroom. (b) Mass acceleration $a$ and bottom force $F$ (the negative sign indicates the compression, not size) versus time for $h_{dh} = 20$ cm. The peak mass acceleration is marked as $a_{peak}$. The peak bottom force is marked as $F_{peak}$. ((c) and (d)) The peak contact stress between the impact mass and the IHPC $\sigma_c = m_{mass}a_{peak}/(\pi r^2_{IHPC})$ and the peak bottom stress $\sigma_f = F_{peak}/(\pi r^2_f)$ versus $h_{dh} = 10$, 20, 30, 40, and 50 cm. The tests are conducted twice with the same IHPC at each drop height.

are the mass and peak acceleration of the impact mass, respectively) between the impact mass and the IHPC to reach the value about 2856N for the drop height $h_{dh} = 20$ cm. But the peak bottom force $F_{peak}$ is about 10N (Fig. 2(b)). After the impact, the mass bounce into the air and the bounced height increases with the drop height. To eliminate the impact of the contact area, we plotted the peak contact stress $\sigma_c$ and the peak bottom stress $\sigma_f$ versus various $h_{dh}$ in Figs. 2(c) and 2(d). The $\sigma_c$ is observed to increase with the drop height in a linear manner over the tested range, and the growth rate is about 9.88 MPa/m. For the $\sigma_f$, the values are not stable at the same drop height, but it slowly increases in average. By comparing these two signals, the scale of $\sigma_c$ is typically about fifty times larger than $\sigma_f$. Furthermore, the growth rate of $\sigma_f$ is faster than $\sigma_c$. These results implicate that the IHPC depress the impact stress transmitting into the bottom storeroom. If the force sensor is substituted by an object, we need to protect, this remarkable performance can protect an object from impact failure.

To clarify how the IHPC can protect the object, the dynamics of the mass are studied. Figs. 3(a) and 3(c) show the mass velocity $V$ and displacement $D$ versus time at various $h_{dh} = 10$, 20, 30, 40, and 50 cm. The dynamic behaviors of the mass included rebound energy $E_b$ and maximal displacement $D_{max}$ are shown in Figs. 3(b) and 3(d). $E_b$ increases with $E_i$ in a linear manner over the tested range, and the bounced energy is about 23% of the impact energy. $D_{max}$ is about 3 mm at $h_{dh} = 10$ cm and maintains the value about 4 mm when $h_{dh}$ over 20 cm. These results have two important implications. First, the IHPC absorbs a part of the impact energy during the impact. And second, the larger the magnitude of the impact is, the harder the IHPC is. It retains the structure integrity of the bottom storeroom and protects the protected object against the region impacted. Thus, energy

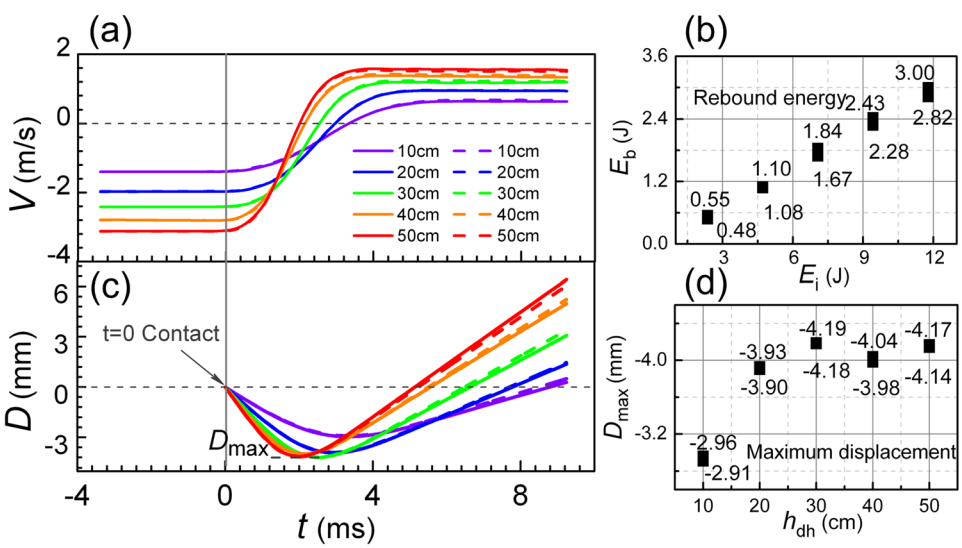


FIG. 3. Dynamics of the impact mass. (a) Mass velocity $V$ versus time. These data are obtained by integrating acceleration-time curves shown in Fig. 2(b). The time $t = 0$ is defined when the impact mass contact the IHPC. Initial mass velocity $V_{t=0} = 0$ satisfy the formula $V_{t=0} = (2gh_{dh})^{1/2}$ (where $g$ is the gravitational acceleration). Rebound velocity of the mass $V_b$ is defined the maximum value in the curve. (b) Rebound energy $E_b = 0.5m_{mass}V^2_b$ versus impact energy $E_i = m_{mass}gh_{dh}$. (c) Mass displacement $D$ versus time for time as shown. These data are obtained by integrating the velocity-time curves shown in Fig. 3(a). (d) Maximum mass displacement $D_{max}$ (negative) versus $h_{dh} = 10$, 20, 30, 40, and 50 cm.

absorption and deformation resistance are the ways how the IHPC protects an object.

These impact behaviors implicate that the mechanical properties of the IHPC are rate dependent. To clarify this, the uniaxial compressive true stress-true strain behaviors[9] of the IHPC were examined at low and high strain rates (Fig. 4(a)). For the low strain rate case (Fig. 4(a) inset), the true stress shows an exponential increase with the true strain. The magnitude of the true stress at the same true strain, as we expected, depends on strain rate. The high strain rate tests ($>1000\,s^{-1}$) are performed on a split Hopkinson pressure bar (SHPB). The complete operation and design details of SHPB techniques for testing of polymeric materials can be found in Ref. 12 and the further description of this SHPB setup see Ref. 13. There are eight strain amplitude regimes and the true stress-true strain is also observed to be rate dependent. (1) The true stress grows linearly as the true strain. The modulus, which defines as the slope of the true stress-strain curve, has a dependence on the strain rate. This is most likely due to the increasing viscous force, which depends on the deformation rate. (2) The stress increase deviate from linear relationship, which known as "anelastic" regimen. (3) The stress reaches the local maximum, and it is called the yield point. After the yield point, the materials enter viscoplasticity regime. (4) Followed by a drop of the stress, it is known as "strain softening." (5) Then, a plastic flow regime characterized by a constant plateau stress appears. (6)The stress grows again, it is known as "strain hardening." The hardening modulus is defined as the slope of the true stress-true strain curves at the region of strain hardening and increases with the strain rate. (7) The stress reaches the second local maximum true stress, and the IHPC start to crack. (8) The crack expands in a large range of strain. After the yield point, the stress keeps nearly constant level over a wide range of strain and it implicates that the IHPC is an excellent energy absorber.[14] Note that only when the strain rate is $14\,132\,s^{-1}$ the IHPC cracks. Below this strain rate, it begins to unloading at the second local maximum true stress.

As seen in a comparison of low and high strain rate (Fig. 4(a)), the true stress at the same true strain can be differed orders of magnitude. To quantify this gap, we plotted the yield stress for high strain rate and the stress at true strain 0.36 for low strain rate versus the natural logarithm of the average true strain rate in Fig. 4(b). The average true strain rate is calculated by $\dot{\varepsilon}_{avg} = \int_0^{\varepsilon_f} \dot{\varepsilon} d\varepsilon / \varepsilon_f$, where $\varepsilon_f$ is the true strain at the fracture point or unloading point. In the high rate, the strain rate effect of the yield stress of the IHPC follows the classic Eyring model $\sigma_y = 40.4\ln(d\varepsilon/dt) - 291.1$. The corresponding stress at the strain rate $0.001\,s^{-1}$ is about $1.07 \times 10^3$ Pa, while the yield stress at the strain rate $14\,132\,s^{-1}$ is about $9.73 \times 10^7$ Pa. The strain rate gives near five orders of magnitude gap for the true stress. According to the mechanical behaviors, the IHPC is most likely in viscous liquid state at the low strain rate. And the eight strain regimes at the high strain rate are the typical behavior of the glassy polymer.[15,16] These results arrive at a conclusion that the IHPC has a phase change when the strain rate is high enough.

As expressed above, the IHPC tested is observed to undergo transition from the viscous liquid state at low rates to the glassy state at high rates. From previous experiments, there is a rubber state between the viscous liquid state and the glassy state of the polymer.[17] Here, an angular frequency $\omega$ versus storage modulus $G'$ behavior was evaluated to obtain the behaviors at the intermediate rate and shows in Fig. 4(c). It is useful to express the frequency dependence as the strain rate dependence, and the equivalent average strain rate can be calculated as, $\dot{\varepsilon}_{avg} = 2\gamma\omega$.[9] The polymer is rubbery when the storage modulus $G'$ reaches a platform of the order about 1 MPa. From the experimental value, the IHPC transit from the viscous liquid state to the rubber state under the angular frequency sweep and diffuse transition angular frequency $\omega_d$ is $12.5\,s^{-1}$. In this scenario, it suggests that the diffuse transition strain rate $\dot{\varepsilon}_d$ is $2.5\,s^{-1}$.

These results describe the process of the phase transitions of the IHPC: (1) viscous liquid state at the low rate, (2)

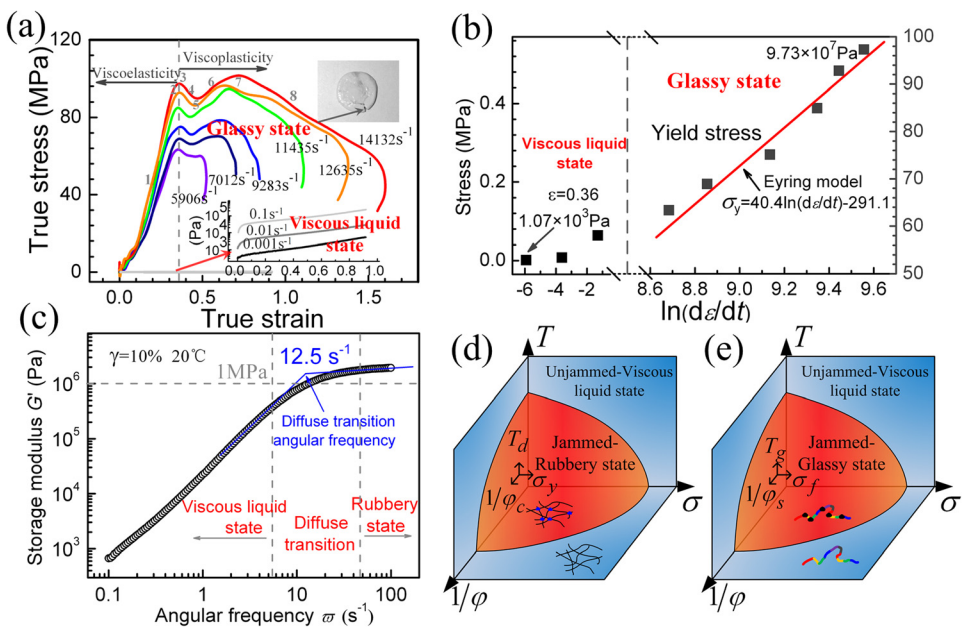


FIG. 4. (a) The true stress versus true strain for the IHPC under high and low strain rate (inset). The low strain rate tests ($<0.1\,s^{-1}$) are performed on a multi-function testing machine (MTS C43.304E) under constant engineering strain rate. (b) Yield stress $\sigma_y$ in the glassy state and stress taken at true strain values of 0.36 in the viscous liquid state versus the natural logarithm of the average true strain rate $\ln(d\varepsilon/dt)$. (c) Angular frequency $\omega$ versus storage modulus $G'$ measured by a torque rheometer (Anton paar, Physica MCR301) with thickness 1 mm. This experiment is conducted at the shear strain $\gamma = 10\%$ and temperature 20 °C. Jamming phase diagrams of the polymer for (d) the diffuse transition and (e) the glassy transition.

rubbery state at the intermediate rate, and (3) glassy state at the high rate. This clarifies why the IHPC has the performance of the energy absorption and deformation resistance. By extension, while the IHPC is struck, the IHPC will be in glassy state which is difficult to deformation. Simultaneously, large amount of energy including stored energy and dissipated energy is absorbed under impact. The stored energy representing the elastic portion, like the rebound energy of the impact mass mentioned above, will be released after impact. The dissipated energy representing the viscous portion dissipates as heat.

The polymer transitions which transited from liquid-like state (viscous liquid state) to solid-like state (rubber state and glassy state) are not caused by chemical reaction, but physical process. These sudden phase transitions conjure images of the jamming field.[18–20] The onset of the liquid-solid transition associated with jamming depends on interplay between temperature $T$, applied stress $\sigma$, and inverse packing faction density $1/\varphi$.[21,22] According to this concept, the falling temperature can jam the liquid-like polymer. Clearly, it is revealed by the previous temperature sweep experiments.[17] The diffuse transition temperature $T_d$ and the glassy transition temperature $T_g$ are defined as the demarcation points of the rubbery and glassy jamming, respectively. The basic difference of rubber state and liquid state is the absence of the holistic movement of the molecular chain and the segments movement is depressed for the glassy state. The raising applied stress can unjam the solid-like polymer, and the system is fluidized. It is usually observed to undergo twice flow behavior after the yield point and the fracture point of the polymer. It is directly measured that the molecular mobility sharply increases at the yield stress.[18] And the molecular dynamics simulations also prove the decrease of entanglement parameter after the yield point.[23] These results show that the yield stress $\sigma_y$ breaks the interaction between the chains and activates the molecular movement. Similarly, the fracture stress $\sigma_f$ breaks the bond and activates the segmental movement.[17,24,25] When the packing density of the chains $\varphi_c$ or the segments $\varphi_s$ reaches the critical points, the polymer at viscous liquid state change to rubber or glass, respectively. As expressed above, the rubbery and glassy jamming could be imaged, as illustrate in Figs. 4(d) and 4(e). In these figures, the jammed states occupy the low-temperature, high-density, and low-stress of the phase diagram and the unjammed state occupy the rest. The interfaces in the three-dimensional space are defined by $T_d$, $1/\varphi_c$, and $\sigma_y$ for the rubbery jamming and $T_g$, $1/\varphi_s$, and $\sigma_f$ for the glassy jamming.

The mechanical property of the polymer depends on the scale of the loading time. This time dependence is due to the rearrangement of the structure (chains and segments) cannot keep pace with the loading time. Two very typical examples are offered by the creep and the relaxation. This implicates that the interaction between the molecular chains or the segments increase at the short experimental time. For example, the entanglements between the chains become physical crosslinking (Figure 4(d) inset). The relative movements of the segments are depressed (Figure 4(e) inset). According to the view of jamming, the critical temperature could decrease by an increase in the attractive interactions.[26] Thus, the phase transition can occur at the room temperature by increasing the strain rate. The jamming model gives another way to build the relationship between the phase transition and microstructure for the polymer. The fundamental similarity between the diffuse/glassy transition and jamming transition should be studied deeply. It is noteworthy that unlike the existing jamming, the molecular size scale, the multiple interactions, and the obvious relaxation process of the polymer could lead to unique behaviors.

In summary, an impact-hardening polymer composite with excellent protective performance is synthesized. By the falling weight tests, we find the protective performance is realized by absorbing a large amount of the impact energy (about 23% of the impact energy stored and a part of impact energy dissipated) and stiffly resisting the deformation (max deformation is about 4 mm). The IHPC transits from viscous fluid state at the low strain rate (measured by the multifunction testing machine) to rubbery state at the intermediate rate (measured by the rheometer) then to glassy state at the high rate (measured by the SHPB) and the diffuse transition strain rate is about $2.5\ s^{-1}$. It is indicated that the phase transitions lead to the deformation resistance and the energy absorption. Finally, an analogy between the jamming and the phase transitions of the polymers are discussed. If these two phenomena are essentially the same, it would provide other research method for polymer science.

Financial support from the National Natural Science Foundation of China (Grant Nos. 11372301, 11125210, and 11102202), the National Basic Research Program of China (973 Program, Grant No. 2012CB937500), and the Anhui Provincial Natural Science Foundation of China (140805QA17) are gratefully acknowledged. The authors also thank Professor Shisheng Hu of USTC and his students for their help on the experiment and useful discussions on the results.

[1]P. J. Hogg, Science **314**, 1100 (2006).
[2]J. H. Lee, D. Veysset, J. P. Singer, M. Retsch, G. Saini, T. Pezeril, K. A. Nelson, and E. L. Thomas, Nat. Commun. **3**, 1164 (2012).
[3]Y. Q. Zhu, T. Sekine, Y. H. Li, W. X. Wang, M. W. Fay, H. Edwards, P. D. Brown, N. Fleischer, and R. Tenne, Adv. Mater. **17**, 1500 (2005).
[4]S. R. Waitukaitis and H. M. Jaeger, Nature **487**, 205 (2012).
[5]V. B. C. Tan, T. E. Tay, and W. K. Teo, Int. J. Solids Struct. **42**, 1561 (2005).
[6]X. L. Gong, Y. L. Xu, W. Zhu, S. H. Xuan, W. F. Jiang, and W. Q. Jiang, J. Compos. Mater. **48**, 641 (2014).
[7]D. Y. Wu, S. Meure, and D. Solomon, Prog. Polym. Sci. **33**, 479 (2008).
[8]J. H. Jang, C. K. Ullal, T. Y. Choi, M. C. Lemieux, V. V. Tsukruk, and E. L. Thomas, Adv. Mater. **18**, 2123 (2006).
[9]J. Yi, M. C. Boyce, G. F. Lee, and E. Balizer, Polymer **47**, 319 (2006).
[10]S. S. Sarva, S. Deschanel, M. C. Boyce, and W. N. Chen, Polymer **48**, 2208 (2007).
[11]R. B. Bogoslovov, C. M. Roland, and R. M. Gamache, Appl. Phys. Lett. **90**, 221910 (2007).
[12]W. Chen, F. Lu, D. J. Frew, and M. J. Forrestal, J. Appl. Mech. **69**, 214 (2002).
[13]W. F. Jiang, X. L. Gong, S. H. Xuan, W. Q. Jiang, F. Ye, X. F. Li, and T. X. Liu, Appl. Phys. Lett. **102**, 101901 (2013).
[14]J. Banhart, Prog. Mater. Sci. **46**, 559 (2001).
[15]K. Chen and K. S. Schweizer, Macromolecules **44**, 3988 (2011).
[16]J. M. Kranenburg, C. A. Tweedie, K. J. van Vliet, and U. S. Schubert, Adv. Mater. **21**, 3551 (2009).
[17]D. W. Van Krevelen, *Properties of Polymers* (Elsevier, Amsterdam 1990).
[18]H. N. Lee, K. Paeng, S. F. Swallen, and M. D. Ediger, Science **323**, 231 (2009).

[19]L. N. Zou, X. Cheng, M. L. Rivers, H. M. Jaeger, and S. R. Nagel, Science **326**, 408 (2009).
[20]C. J. O. Reichhardt and L. M. Lopatina, Science **326**, 374 (2009).
[21]A. J. Liu and S. R. Nagel, Nature **396**, 21 (1998).
[22]Z. X. Zhang, N. Xu, D. T. N. Chen, P. Yunker, A. M. Alsayed, K. B. Aptowicz, P. Habdas, A. J. Liu, S. R. Nagel, and A. G. Yodh, Nature **459**, 230 (2009).
[23]D. Hossain, M. A. Tschopp, D. K. Ward, J. L. Bouvard, P. Wang, and M. F. Horstemeyer, Polymer **51**, 6071 (2010).
[24]K. Chen and K. S. Schweizer, Phys. Rev. Lett. **102**, 038301 (2009).
[25]T. Barany, T. Czigany, and J. Karger-Kocsis, Prog. Polym. Sci. **35**, 1257 (2010).
[26]V. Trappe, V. Prasad, L. Cipelletti, P. N. Segre, and D. A. Weitz, Nature **411**, 772 (2001).